DOI:10.11973/jxgccl240174

道间温度与焊后热处理冷却速率对 P91 钢焊缝金属冲击韧性与耐腐蚀性能的影响

徐晓龙[1],李文清[2],刘梓申[2],杨 飞[1],毛兴贵[1],蒋 勇[1]
(1. 四川大西洋焊接材料股份有限公司,自贡 643000;2. 兰州理工大学材料科学与工程学院,省部共建有色金属先进加工与再利用国家重点实验室,兰州 730050)

摘 要:在不同道间温度(250,300 ℃)下对P91钢进行8层16道埋弧焊,并对焊缝金属进行760 ℃×2 h焊后热处理,冷却速率分别为55 ℃·h^{-1}和约20 ℃·h^{-1}(随炉冷却),研究了道间温度与焊后热处理冷却速率对焊缝金属冲击韧性和耐腐蚀性能的影响。结果表明:当道间温度为250 ℃时,随着焊后热处理冷却速率由约20 ℃·h^{-1}提高到55 ℃·h^{-1},焊缝金属晶界处碳化物含量及其聚集程度降低,冲击吸收能量明显提高(幅度约68%),波动程度明显降低,自腐蚀电位提高,自腐蚀电流密度降低;当焊后热处理冷却速率约为20 ℃·h^{-1}时,随着道间温度由250 ℃升高到300 ℃,碳化物含量及其聚集程度降低,冲击吸收能量略微提高,波动程度略微降低,自腐蚀电位提高,自腐蚀电流密度降低。在试验参数范围内,P91钢埋弧焊的道间温度和焊后热处理冷却速率应分别控制在250 ℃和55 ℃·h^{-1},此时焊缝金属的冲击吸收能量最大,其波动程度最小,自腐蚀电位最大,自腐蚀电流密度最小,冲击韧性和耐腐蚀性能最优。

关键词:P91耐热钢;埋弧焊;焊后热处理;冲击韧性;碳化物;耐腐蚀性能
中图分类号:TG407 **文献标志码**:A **文章编号**:1000-3738(2025)03-0041-08

0 引 言

铬钼系耐热钢广泛应用于现代火力发电厂,其在高温下具有优异的抗蠕变性能、耐腐蚀性能、耐应力腐蚀开裂性能以及低热膨胀系数。其中,P91耐热钢是介于2.25Cr-1Mo低合金钢和奥氏体不锈钢之间的改良型9Cr-1Mo马氏体耐热钢[1],相比较于传统的耐热钢,具有更优异的高温强度、抗氧化性能和抗蠕变性能[2-3]。在实际应用中,P91钢存在焊缝金属冲击韧性差和不稳定的问题。焊接工艺与焊后热处理制度通过影响焊缝金属的组织及析出相形貌和种类等,对其冲击韧性与耐腐蚀性能产生显著影响[4],相关研究很多[5-6]。焊接道间温度和焊后热处理冷却速率对焊缝金属力学性能和耐腐蚀性有显著影响。鲁克莹等[7]研究发现,若不控制道间温度,则16MnDR钢焊缝金属的冲击韧性下降。周勇等[8]研究发现,随着道间温度的升高,R307耐热钢焊缝金属的强度降低,冲击韧性先升后降。杜吉康等[9]研究发现,降低焊后热处理冷却速率可以显著减少U75V钢焊缝金属中的马氏体含量。谢少辉等[10]研究发现,610~630 ℃焊后热处理后的空冷相较于炉冷更有利于避免高强钢焊缝金属的脆化。目前,有关焊后热处理冷却速率和道间温度对P91钢焊缝金属组织和性能影响的研究较少[11-12]。为此,作者在不同道间温度下对P92钢进行多层多道埋弧焊,然后对焊缝金属进行不同冷却速率下的760 ℃×2 h焊后热处理,研究了不同道间温度与焊后热处理冷却速率下焊缝金属的冲击韧性和耐腐蚀性能,以期为P92钢焊接工艺和焊后热处理工艺的制定提供理论指导。

1 试样制备与试验方法

试验材料为P91钢,焊接材料为埋弧焊焊丝/焊剂CHF91/CHW-SB91,二者均由四川大西洋焊接材料股份有限公司提供。按照GB/T 25774.1—2010《焊接材料的检验 第1部分:钢、镍及镍合金熔敷金属力学性能试样的制备及检验》制备熔覆金属力学

收稿日期:2024-04-02;**修订日期**:2025-01-06
基金项目:甘肃省拔尖领军人才项目;中央引导地方科技发展专项项目(24ZYQA054);甘肃省重点研发计划项目(23YFGA0057);国家自然科学基金资助项目(52175325,51961024,52071170);甘肃省科技重大专项项目(23ZDGA010,22ZD6GA008)
作者简介:徐晓龙(1988—),男,四川达州人,高级工程师,硕士

性能试样,试样尺寸为350 mm×150 mm×20 mm,根部间隙为16 mm,坡口角度为10°,焊接时采用垫板。采用MZ-1000IV型逆变式直流埋弧焊机进行8层16道焊,焊接接头的具体结构如图1所示,焊接电压为30 V,焊接电流为420~450 A,焊接速度控制在38~40 cm·min^{-1},通过红外测温仪控制道间温度,层间与道间停留时间根据道间温度控制。焊接完成后对试样进行760 ℃×2 h焊后热处理,道间温度和焊后热处理冷却速率见表1。通过光谱法测得焊缝金属的化学成分如表2所示。

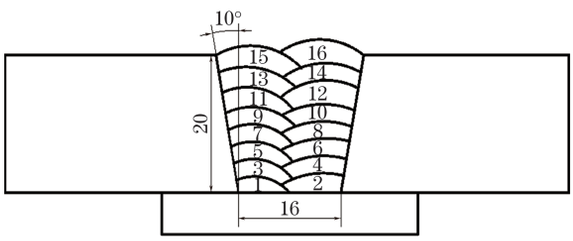

图1 焊接接头结构示意

Fig. 1 Schematic of welded joint structure

表1 道间温度和焊后热处理冷却速率

Table 1 Interpass temperature and cooling rate of post-weld heat treatment

编号	道间温度/℃	焊后热处理冷却速率/(℃·h^{-1})
1	250	55
2	250	约20(随炉冷却)
3	300	约20(随炉冷却)

按照GB/T 229—2020《金属材料 夏比摆锤冲击试验方法》,在熔覆金属力学性能试样的板厚中间位置以焊缝为中心垂直于焊接方向截取冲击试样,冲击试样的尺寸为55 mm×10 mm×10 mm,V型缺口开在试样中心的焊缝金属处,缺口深度为2 mm,缺口夹角为45°,采用PTMS4450型摆锤冲击试验机在20 ℃下进行夏比冲击试验。采用TESCAN MIRA3型场发射扫描电镜(SEM)对断口形貌进行观察,通过Image软件确定焊缝金属裂纹源的位置,用线切割机在断口裂纹源位置垂直于缺口方向进行切割,对切割横截面进行打磨、抛光,用体积分数10%硝酸乙醇溶液腐蚀后,采用SEM观察裂纹源附近的微观结构,并用其附带的能谱仪(EDS)进行微区成分分析。在焊缝金属中心位置截取尺寸为10 mm×10 mm×5 mm的电化学腐蚀试样,除测试面外,其余面用环氧树脂密封。采用CHI600D型电化学工作站使用三电极体系进行极化曲线的测试,电化学腐蚀试样作为工作电极,铂电极作为辅助电极,饱和甘汞电极(SCE)作为参比电极,电解液为质量分数3.5%的NaCl溶液。将工作电极在电解液中静置2 000 s,测量开路电位。极化曲线测试时的扫描速率为0.5 mV·s^{-1},动电位扫描范围为−0.1~0.1 V,测试温度为室温。

表2 焊缝金属的化学成分

Table 2 Chemical composition of weld metal

元素	C	Mn	Si	Cr	Ni	Mo	V	N	Nb	Fe
质量分数/%	0.082	0.55	0.078	8.52	0.63	0.90	0.17	0.035	0.029	余

2 试验结果与讨论

2.1 冲击韧性

当道间温度固定为250 ℃时,55 ℃·h^{-1}焊后热处理冷却速率下焊缝金属的冲击吸收能量测试值为119,94,105,109,114 J,平均值为(108.2±9.42)J;约20 ℃·h^{-1}焊后热处理冷却速率下的测试值为45,65,45,62,105 J,平均值为(64.4±24.53)J。300 ℃道间温度和约20 ℃·h^{-1}焊后热处理冷却速率下焊缝金属的冲击吸收能量测试值为76,60,77,71,45 J,平均值为(65.8±13.44)J。可见,当道间温度固定为250 ℃时,随着焊后热处理速率由约20 ℃·h^{-1}增加到50 ℃·h^{-1},焊缝金属的冲击吸收能量明显提高,幅度约为68%,波动程度明显降低;当焊后热处理冷却速率固定为约20 ℃·h^{-1}时,随着道间温度由250 ℃升高到300 ℃,冲击吸收能量略微提高,波动程度略微降低。在250 ℃道间温度和55 ℃·h^{-1}焊后热处理冷却速率下,焊缝金属的冲击吸收能量最高并且波动程度最小。

由图2~图4可以看出:当道间温度固定为250 ℃时,与约20 ℃·h^{-1}焊后热处理冷却速率下相比,55 ℃·h^{-1}焊后热处理冷却速率下焊缝金属的冲击断口更粗糙,裂纹源位置距缺口根部的位置更远,塑性裂纹扩展长度更长;55 ℃·h^{-1}焊后热处理冷却速率下焊缝金属的冲击断裂形式以韧性断裂或韧脆混合断裂为主,而约20 ℃·h^{-1}焊后热处理冷却速率下的冲击断裂形式以解理断裂为主。在300 ℃道间温度和约20 ℃·h^{-1}焊后热处理冷却速率下焊缝金属

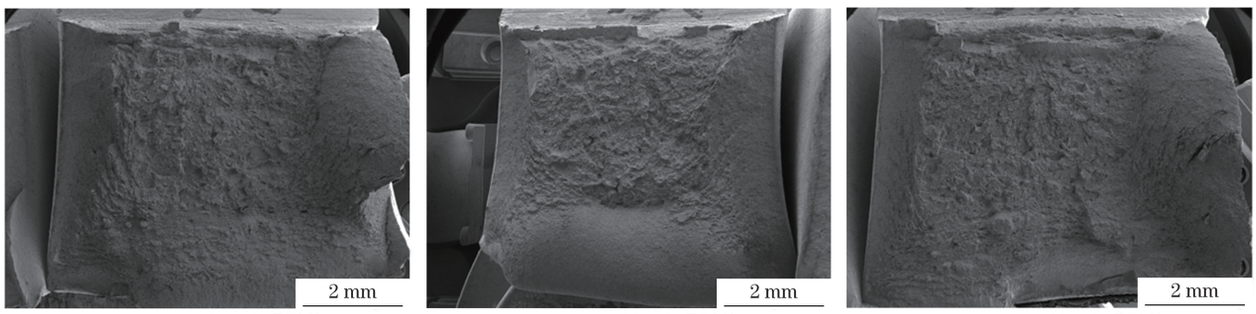

(a) 119 J，断口宏观形貌　(b) 94 J，断口宏观形貌　(c) 105 J，断口宏观形貌

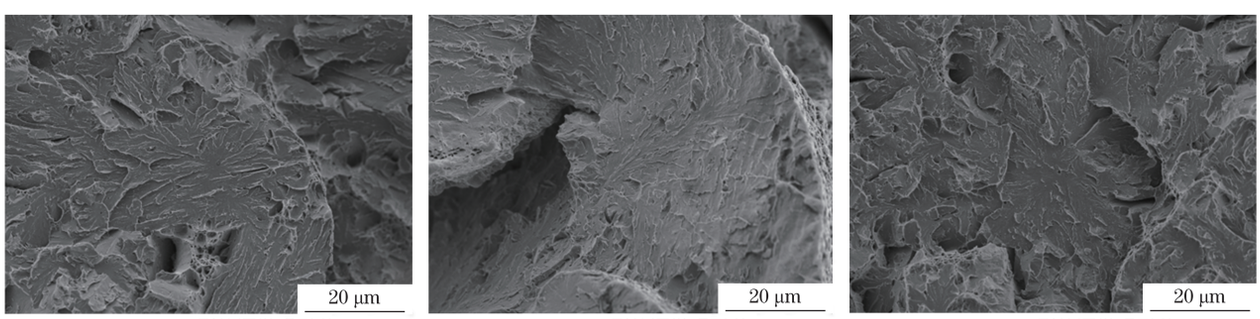

(d) 119 J，裂纹源微观形貌　(e) 94 J，裂纹源微观形貌　(f) 105 J，裂纹源微观形貌

图 2　55 ℃·h^{-1} 焊后热处理冷却速率下不同冲击吸收能量的焊缝金属断口宏观形貌与裂纹源微观形貌 (道间温度 250 ℃)

Fig. 2　Fracture macromorphology (a–c) and crack initiation source micromorphology (d–f) of weld metal with different impact absorbed energies at post-weld heat treatment cooling rate of 55 ℃·h^{-1} (interpass temperature of 250 ℃)

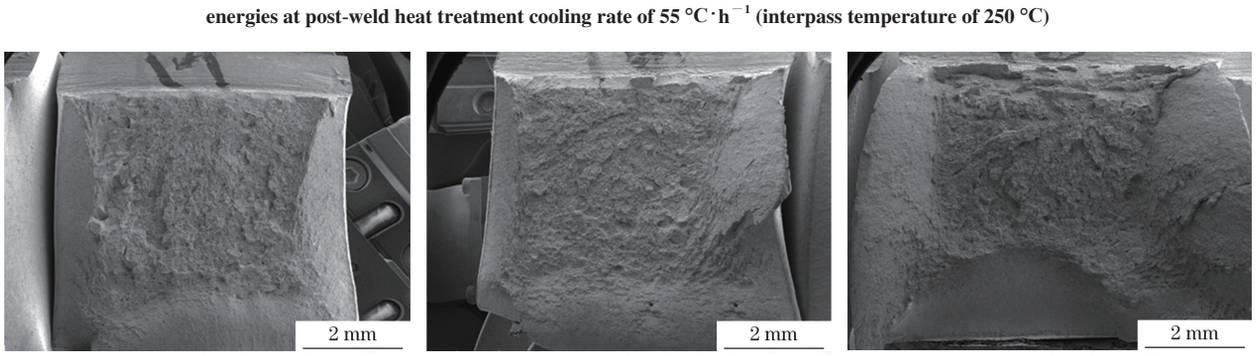

(a) 45 J，断口宏观形貌　(b) 65 J，断口宏观形貌　(c) 105 J，断口宏观形貌

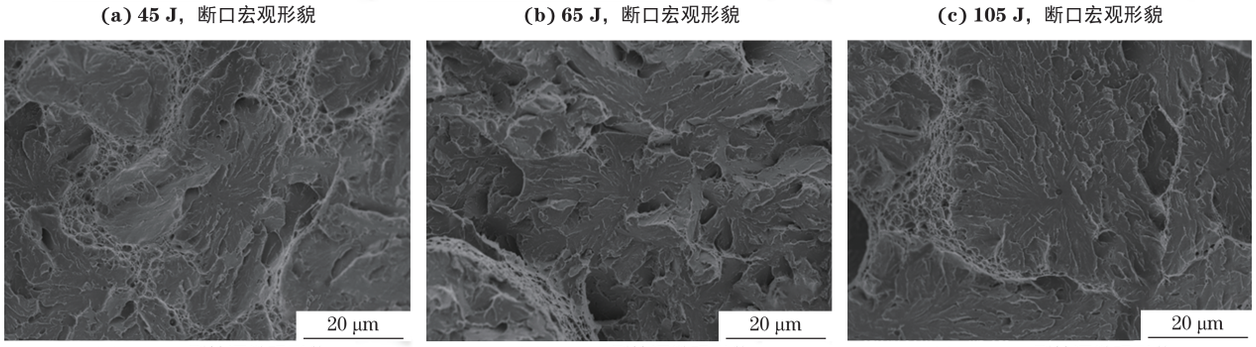

(d) 45 J，裂纹源微观形貌　(e) 65 J，裂纹源微观形貌　(f) 105 J，裂纹源微观形貌

图 3　约 20 ℃·h^{-1} 焊后热处理冷却速率下不同冲击吸收能量的焊缝金属断口宏观形貌与裂纹源微观形貌 (道间温度 250 ℃)

Fig. 3　Fracture macromorphology (a–c) and crack initiation source micromorphology (d–f) of weld metal with different impact absorbed energies at post-weld heat treatment cooling rate of about 20 ℃·h^{-1} (interpass temperature of 250 ℃)

起裂源距缺口根部非常近,断口存在韧窝和解理面,断裂形式为韧脆混合断裂。综上,在250 ℃道间温度和55 ℃·h^{-1}焊后热处理冷却速率下焊缝金属的冲击性能更好。

由图5可以看出,55 ℃·h^{-1}焊后热处理冷却速率下,不同冲击吸收能量的焊缝金属裂纹源附近的基体组织均为铁素体,其晶界和晶内存在少量链状碳化物,且晶界处未观察到碳化物颗粒聚集的现象。由图6可知:约20 ℃·h^{-1}焊后热处理冷却速率下,焊缝金属裂纹源附近基体组织也均为铁素体。其中:

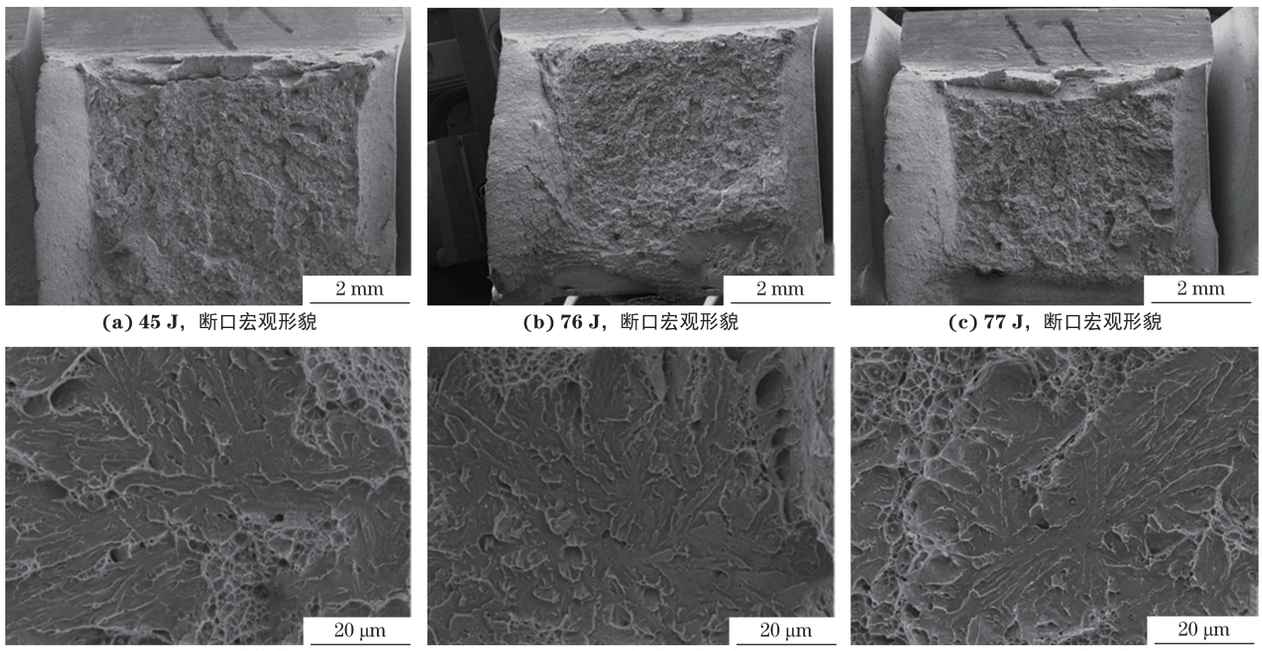

(a) 45 J，断口宏观形貌　(b) 76 J，断口宏观形貌　(c) 77 J，断口宏观形貌

(d) 45 J，裂纹源微观形貌　(e) 76 J，裂纹源微观形貌　(f) 77 J，裂纹源微观形貌

图 4　300 ℃道间温度和约 20 ℃·h^{-1}焊后热处理冷却速率下不同冲击吸收能量的焊缝金属断口宏观形貌与裂纹源微观形貌

Fig. 4　Fracture macromorphology (a–c) and crack initiation source micromorphology (d–f) of weld metal with different impact absorbed energies at interpass temperatures of 300 °C and post-weld heat treatment cooling rate of about 20 °C·h^{-1}

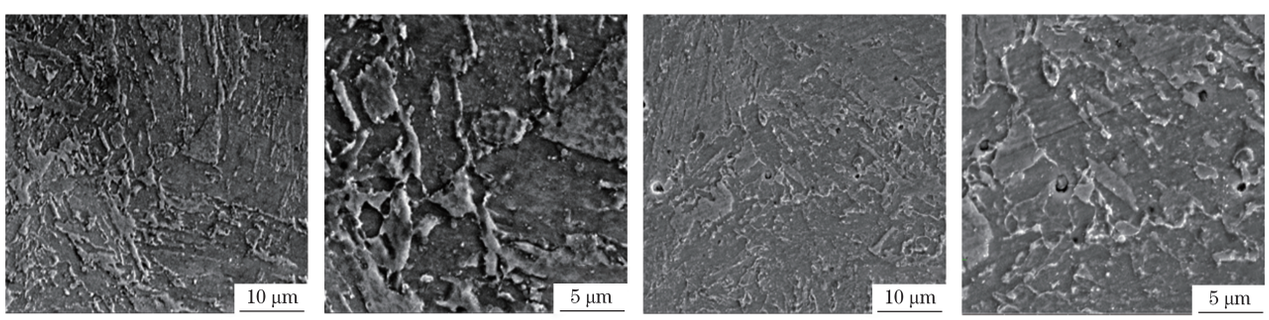

(a) 119 J，低倍　(b) 119 J，高倍　(c) 105 J，低倍　(d) 105 J，高倍

图 5　55 ℃·h^{-1}焊后热处理冷却速率下不同冲击吸收能量的焊缝金属裂纹源附近的微观形貌(道间温度 250 ℃)

Fig. 5　Micromorphology near crack initiation source of weld metal with different impact absorbed energies at post-weld heat treatment cooling rate of 55 °C·h^{-1} (interpass temperature of 250 °C) : (a, c) at low magnification and (b, d) at high magnification

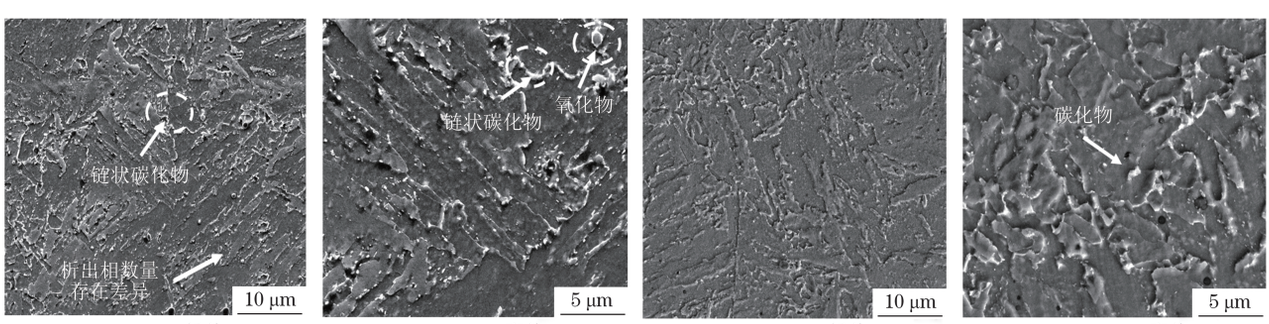

(a) 45 J，低倍　(b) 45 J，高倍　(c) 105 J，低倍　(d) 105 J，高倍

图 6　约 20 ℃·h^{-1}焊后热处理冷却速率下不同冲击吸收能量的焊缝金属裂纹源附近的微观形貌(道间温度 250 ℃)

Fig. 6　Micromorphology near crack initiation source of weld metal with different impact absorbed energies at post-weld heat treatment cooling rate of about 20 °C·h^{-1} (interpass temperature of 250 °C): (a, c) at low magnification and (b, d) at high magnification

45 J冲击吸收能量的焊缝金属组织中观察到大量碳化物,且晶界处的碳化物发生聚集,与55 ℃·h^{-1}焊后热处理冷却速率下相比,碳化物数量明显增加;105 J冲击吸收能量的焊缝金属组织中碳化物较少,

未出现聚集现象,与55 ℃·h^{-1}焊后热处理冷却速率下的组织相似。造成不同焊后热处理冷却速率下焊缝金属冲击韧性和冲击吸收能量波动性差异的主要原因在于组织中碳化物的含量以及晶界碳化物的聚集程度。较快的焊后热处理冷却速率会导致焊缝中的碳化物来不及析出,因此碳化物析出数量少;反之,碳化物充分析出,组织中碳化物数量大量增加,并造成碳化物的聚集。

由图7可以看出,300 ℃道间温度和约20 ℃·h^{-1}焊后热处理冷却速率下焊缝金属裂纹源附近的基体组织为铁素体,同时还存在链状碳化物,晶界碳化物未出现明显聚集现象,能谱分析表明该碳化物主要为富铬、锰的碳化物。当焊后热处理冷却速率约为20 ℃·h^{-1}时,与250 ℃道间温度相比,300 ℃道间温度下焊缝金属的碳化物含量较少,且晶界碳化物未出现明显聚集现象。与250 ℃道间温度和55 ℃·h^{-1}焊后热处理冷却速率下相比,300 ℃道间温度和约20 ℃·h^{-1}焊后热处理冷却速率下碳化物含量有所增加。经焊后760 ℃热处理后,较低道间温度的焊缝金属组织中的碳化物在晶界处重新形核、长大[13-16],呈聚集状态;较高道间温度的焊缝金属组织中的晶界处碳化物的生长受到抑制[17],碳化物未见明显聚集现象。因此,道间温度较高的焊缝金属的冲击韧性更好,冲击吸收能量波动性更低。

2.2 耐腐蚀性能

由图8可知,不同道间温度和焊后热处理冷却速率下焊缝金属的极化曲线形状基本相同,仅位置发生偏移。

自腐蚀电流密度越小,腐蚀率越小,材料的耐腐蚀性能越好;自腐蚀电位越小,材料越易腐蚀[18]。由表3可知:250 ℃道间温度和55 ℃·h^{-1}焊后热处理冷却速率下焊缝金属的自腐蚀电位最大,自腐蚀电流密度最小,说明此时焊缝金属的耐腐蚀性能最好;250 ℃道间温度和约20 ℃·h^{-1}焊后热处理冷却速率下的自腐蚀电位最小,自腐蚀电流密度最大,说明此时焊缝金属的耐腐蚀性能最差。焊缝金属的耐腐蚀性能与其组织中晶界处析出相的聚集程度有关。由前文组织分析可知,P91钢焊缝金属晶界处聚集着大量链状的富铬、锰的碳化物颗粒;富铬相的析出使得晶界处形成贫铬区[19],贫铬区与非贫铬区形成大量的原电池,导致晶界贫铬区优先发生腐蚀。晶界富铬相的聚集程度越大,形成的贫铬区域越大,腐蚀程度越大,耐腐蚀性能越差。250 ℃道间温度和55 ℃·h^{-1}焊后热处理冷却速率下焊缝金属晶界处碳化物聚集程度最低,未出现链状碳化物在晶界上聚集的现象,因此耐腐蚀性能最好;250 ℃道

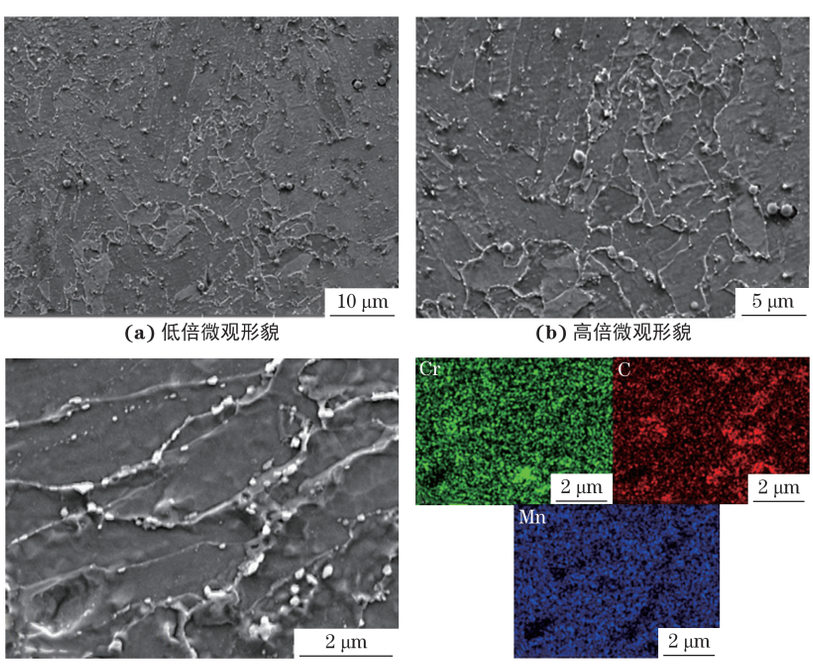

(a) 低倍微观形貌 (b) 高倍微观形貌

(c) 面扫描位置 (d) 面扫描结果

图7 300 ℃道间温度和约20 ℃·h^{-1}焊后热处理冷却速率下焊缝金属裂纹源附近的微观形貌及EDS面扫描位置和结果(冲击吸收能量76 J)

Fig. 7 Micromorphology (a–b) and EDS surface scan position (c) and results (d) near crack initiation source of weld metal at interpass temperature of 300 °C and post-weld heat treatment cooling rate of about 20 °C·h^{-1} (impact absorbed energy of 76 J): (a) at low magnification and (b) at high magnification

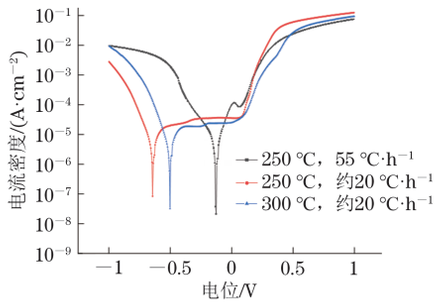

图 8　不同道间温度和焊后热处理冷却速率下的焊缝金属在 NaCl 溶液中的极化曲线

Fig. 8　Polarization curves of weld metal in NaCl solution at different interpass temperatures and post-weld heat treatment cooling rates

表 3　不同道间温度和焊后热处理冷却速率下焊缝金属的电化学参数

Table 3　Electrochemical parameters of weld metal at different interpass temperatures and post-weld heat treatment cooling rates

道间温度/℃	焊后热处理冷却速率/(℃·h^{-1})	自腐蚀电位/V	自腐蚀电流密度/(A·cm^{-2})
250	55	−0.126	2.098×10^{8}
250	约20	−0.644	8.417×10^{8}
300	约20	−0.502	3.207×10^{8}

间温度和约20 ℃·h^{-1}焊后热处理冷却速率下晶界处链状碳化物大量聚集,导致出现大量贫铬区,因此耐腐蚀性能最差;300 ℃道间温度和约20 ℃·h^{-1}焊后热处理冷却速率下的碳化物聚集程度低于250 ℃道间温度和约20 ℃·h^{-1}焊后热处理冷却速率,但高于250 ℃道间温度和55 ℃·h^{-1}焊后热处理冷却速率下,因此焊缝金属的耐腐蚀性能介于二者之间。

3　结　论

(1)当道间温度为250 ℃时,随着焊后热处理冷却速率由约20 ℃·h^{-1}提高到55 ℃·h^{-1},焊缝金属晶界处碳化物含量和聚集程度降低,冲击吸收能量明显提高,幅度约为68%,波动程度明显降低,冲击韧性变好;当焊后热处理冷却速率约为20 ℃·h^{-1}时,随着道间温度由250 ℃升高到300 ℃,碳化物含量及聚集程度降低,冲击吸收能量略微提高,波动程度略微降低,冲击韧性变好。

(2)当道间温度为250 ℃时,随着焊后热处理冷却速率由约20 ℃·h^{-1}提高到55 ℃·h^{-1},自腐蚀电位提高,自腐蚀电流密度降低,耐腐蚀性能提高;当焊后热处理冷却速率约为20 ℃·h^{-1}时,随着道间温度由250 ℃升高到300 ℃,自腐蚀电位提高,自腐蚀电流密度降低,耐腐蚀性能提高。

(3)在试验参数范围内,P91钢埋弧焊的道间温度和焊后热处理冷却速率应分别控制在250 ℃和55 ℃·h^{-1},此时焊缝金属的冲击韧性和耐腐蚀性能最优。

参考文献:

[1] 宿修平,苏德瑞. P91钢焊缝缺陷检测及原因探讨[J]. 华北电力技术,2006(7):44-47.
SU X P, SU D R. Detection and study on welded seam defects of P91 steel[J]. North China Electric Power, 2006(7):44-47.

[2] SAINI N, PANDEY C, MAHAPATRA M M, et al. A comparative study of ductile-brittle transition behavior and fractography of P91 and P92 steel[J]. Engineering Failure Analysis, 2017, 81:245-253.

[3] SILVA F J G, PINHO A P, PEREIRA A B, et al. Evaluation of welded joints in P91 steel under different heat-treatment conditions[J]. Metals, 2020, 10(1):99.

[4] PANDEY C, GIRI A, MAHAPATRA M M. Evolution of phases in P91 steel in various heat treatment conditions and their effect on microstructure stability and mechanical properties[J]. Materials Science and Engineering: A, 2016, 664:58-74.

[5] LI J R, ZHANG C L, LIU Y Z. Influence of carbides on the high-temperature tempered martensite embrittlement of martensitic heat-resistant steels[J]. Materials Science and Engineering: A, 2016, 670:256-263.

[6] 李文清,曹睿,杨飞,等. 影响P91耐热钢焊缝金属冲击韧性的因素分析[J]. 材料导报,2024,38(3):147-151.
LI W Q, CAO R, YANG F, et al. Analysis of factors affecting the impact toughness of P91 heat-resistant steel weld metal[J]. Materials Reports, 2024, 38(3):147-151.

[7] 鲁克莹,董俊军,王建才,等. 道间温度对焊接接头力学性能的影响[J]. 焊接技术,2023,52(11):124-128.
LU K Y, DONG J J, WANG J C, et al. Effect of interpass temperature on mechanical properties of welded joints[J]. Welding Technology, 2023, 52(11):124-128.

[8] 周勇,汪选国,宋昌宝. 道间温度对耐热钢焊条熔敷金属微观组织和力学性能的影响[J]. 金属热处理,2017,42(8):131-135.
ZHOU Y, WANG X G, SONG C B. Effect of interpass temperature on microstructure and mechanical properties of deposited metal of heat resistant steel electrode[J]. Heat Treatment of Metals, 2017, 42(8):

131-135.

[9] 杜吉康,詹新伟,王树青. U75V钢轨闪光焊焊后热处理冷却工艺优化研究[J]. 高速铁路新材料,2022,1(6):47-52.
DU J K, ZHAN X W, WANG S Q. Research on optimization of cooling process in the post-weld heat treatment of U75V rails flash butt welding joints[J]. Advanced Materials of High Speed Railway, 2022, 1(6): 47-52.

[10] 谢少辉,尹士科. 高强度焊缝焊后热处理参数的确定[J]. 焊接技术,2004,33(4):18-19.
XIE S H, YIN S K. Determination of postweld heat treatment parameters of high strength weld[J]. Welding Technology, 2004, 33(4): 18-19.

[11] WANG Y Y, KANNAN R, LI L J. Characterization of as-welded microstructure of heat-affected zone in modified 9Cr-1Mo-V-Nb steel weldment[J]. Materials Characterization, 2016, 118: 225-234.

[12] ŽUŽEK B, PODGORNIK B, KAFEXHIU F. Development of microstructure and creep resistance of a martensitic creep resistant steel[J]. International Journal of Microstructure and Materials Properties, 2017, 12(3/4): 301.

[13] YU X, BABU S S, TERASAKI H, et al. Correlation of precipitate stability to increased creep resistance of Cr-Mo steel welds[J]. Acta Materialia, 2013, 61(6): 2194-2206.

[14] 张群兵,牛靖,赵鹏飞,等. 预热温度对12Cr10Co3W2Mo耐热钢焊接冷裂纹敏感性的影响[J]. 焊接学报,2015,36(4):87-91.
ZHANG Q B, NIU J, ZHAO P F, et al. Influence of preheating temperature on cold cracking sensitivity of 12Cr10Co3W2Mo heat resistant steel[J]. Transactions of the China Welding Institution, 2015, 36(4): 87-91.

[15] FRANCIS J A, CANTIN G M D, MAZUR W, et al. Effects of weld preheat temperature and heat input on type IV failure[J]. Science and Technology of Welding and Joining, 2009, 14(5): 436-442.

[16] SETHI A K. Studies on hard surfacing of structural steel by gas thermal spraying process[J]. Materials Today: Proceedings, 2020, 21: 1436-1440.

[17] 李文清,马景平,曹睿,等. P91钢焊缝金属碳化物聚集程度的差异对焊缝金属冲击韧性的影响[J]. 材料导报,2024,38(20):202-208.
LI W Q, MA J P, CAO R, et al. Effect of different degree of carbide aggregation in P91 steel weld metal on the impact toughness of weld metal[J]. Materials Reports, 2024, 38(20): 202-208.

[18] 曹飞杨,谢敬佩,王淼辉,等. 喷射成形H13钢的耐腐蚀行为[J]. 材料热处理学报,2016,37(1):163-168.
CAO F Y, XIE J P, WANG M H, et al. Corrosion behavior of sprayed-formed H13 steel[J]. Transactions of Materials and Heat Treatment, 2016, 37(1): 163-168.

[19] 缪乐德,张毅,杨建强,等. 不同热处理状态下镍基耐蚀合金析出相的定性定量分析[J]. 冶金分析,2015,35(1):6-12.
MIAO L D, ZHANG Y, YANG J Q, et al. Qualitative and quantitative analysis of precipitate phases in nickel-based corrosion resistant alloys with different isothermal situation[J]. Metallurgical Analysis, 2015, 35(1): 6-12.

Effects of Interpass Temperature and Post-Weld Heat Treatment Cooling Rate on Impact Toughness and Corrosion Resistance of P91 Steel Weld Metal

XU Xiaolong[1], LI Wenqing[2], LIU Zishen[2], YANG Fei[1], MAO Xinggui[1], JIANG Yong[1]

(1. Atlantic China Welding Consumables, INC, Zigong 643000, China; 2. The State Key Laboratory of Advanced Processing and Recycling of Nonferrous Metals, School of Materials Science and Engineering, Lanzhou University of Technology, Lanzhou 730050, China)

Abstract: P91 steel was subjected to 8-layer 16-pass submerged arc welding at different interpass temperatures (250, 300 ℃), and the weld metal was post-weld heated at 760 ℃ for 2 h at cooling rates of 55 ℃·h^{-1} and about 20 ℃·h^{-1} (furnace cooling). The effects of interpass temperature and post-weld heat treatment cooling rate on the impact toughness and corrosion resistance of weld metal were studied. The results show that when the interpass temperature was 250 ℃, with post-weld heat treatment cooling rate increasing from about 20 ℃·h^{-1} to 55 ℃·h^{-1}, the carbide content and its aggregation degree at grain boundaries of the weld metal decreased, the impact absorbed energy obviously increased by about 68%, and its fluctuation degree obviously decreased; the free-corrosion potential increased, and the free-corrosion current density decreased. When the post-welding heat treatment cooling rate was about 20 ℃·h^{-1}, with the interpass temperature increasing from 250 ℃ to 300 ℃, the carbide content and its aggregation degree decreased, the impact absorbed energy slightly increased, and its fluctuation degree slightly decreased; the free-corrosion potential increased, and the free-corrosion current density decreased. Within the range of test parameters, the interpass temperature and the post-weld heat treatment cooling rate of submerged arc welding of P91 steel should be controlled at 250 ℃, 55 ℃·h^{-1}, respectively; at this time the weld metal had the largest impact absorbed energy and free-corrosion potential and the smallest fluctuation of impact absorbed energy and free-corrosion current density, and the impact toughness and corrosion resistance were the best.

Key words: P91 heat resistant steel; submerged arc welding; post-weld heat treatment; impact toughness; carbide; corrosion resistance

(上接第19页)

View of EVI Mode in Automotive Material Research & Development and Promoting Application

MA Mingtu[1], LU Hongzhou[2], ZHAO Yan[3], FENG Yi[1], WANG Guangyao[1], LI Bo[4], YUAN Guo[5], MIAO Xinlei[6], MENG Jing[6]

(1. China Automotive Engineering Research Institute Co., Ltd., Chongqing 401121, China; 2. CITIC Metals Co., Ltd., Beijing 100004, China; 3. Chongqing Innovation Center of Beijing Institute of Technology, Chongqing 401120, China; 4. Sino-US (Chongqing) Super High Strength Material Research Institute Co., Ltd., Chongqing 401120, China; 5. State Key Laboratory of Steel Rolling Technology and Continuous Rolling Automation, Northeastern University, Shenyang 110819, China; 6. Ansteel ThyssenKrupp Automotive Steel Co., Ltd., Dalian 116600, China)

Abstract: Early vendor involvement (EVI) mode in the research & development and promoting application of automotive materials is discussed in detail. The background and connotation of the development of this mode and the important role in the research & development and application of new materials are introduced. The EVI activities and characteristics of some well-known companies at home and abroad are introduced in detail, as well as the recent achievements of TAGAL in the digital body platform and its steel solutions are introduced. The progress of EVI promotion activities by relevant enterprises is introduced. The role of EVI mode in the application of new materials in newly developed vehicle models is discussed, and the conditions for enterprises to promote the application of EVI mode are put forward. Finally, the significance of EVI model to dual-carbon strategy is expounded.

Key words: EVI mode; research & development and application of new material; benchmarking car; concept car